Nonlinear dynamics of superparamagnetic beads in a traveling magnetic-field wave

Benjamin B. Yellen and Lawrence N. Virgin
Department of Mechanical Engineering and Materials Science, Duke University, Durham, North Carolina 27708, USA
Center for Biologically Inspired Materials and Material Systems (CBIMMS), Duke University, Durham, North Carolina 27708, USA
and Department of Civil and Environmental Engineering, Duke University, Durham, North Carolina 27708, USA
(Received 26 March 2009; published 6 July 2009)

The nonlinear dynamic behavior of superparamagnetic beads exposed to a periodic array of micromagnets and an external rotating field is simulated as a function of the relative size of the bead with respect to the micromagnet size and the strength of the external field relative to the pole density of the substrate. For large bead sizes, it is confirmed that the motion of the beads corresponds to the dynamics of an overdamped nonlinear harmonic oscillator. For lower bead sizes, additional subharmonic locking effects are observed along with the emergence of bounded orbits. These results qualitatively support previous experimental investigations of traveling-wave magnetophoresis and provide guidelines for achieving nearly infinite separation resolution between differently sized beads.

DOI: 10.1103/PhysRevE.80.011402 PACS number(s): 82.70.Dd, 05.45.−a, 64.75.Xc

I. INTRODUCTION

The motion of objects through periodic potential-energy landscapes has been observed in a number of physical systems, including atom migration on crystal surfaces [1], the motion of charge-density packets in crystals and fluids [2,3], the movement of vortices in type II superconductors [4], fluid driven movement of colloidal particles through optical lattices [5–7], as well as various problems in chemical kinetics [8]. Transportation of objects by translating periodic potential-energy landscapes has also been studied extensively at the macroscales and microscales. At the macroscale, traveling field waves are the basis for operation of electric trains [9] and newer magnetic levitation trains [10], and even certain types of roller coasters. At the microscale, traveling field waves are used to transport microsized and nanosized colloidal particles using electric [11,12], optical [5,13], magnetic [14–16], or acoustic fields [17]. In this regard, most attention has been paid to the phase-locked regime of motion, where the bead is forced to move at the same speed as the traveling wave; while significantly less attention has been paid to the phase-slipping regime of motion, which has potential applications in size sorting and biological separation. For example, Yellen *et al.* experimentally demonstrated that nearly infinite separation resolution between two different types of magnetic beads can be achieved by exploiting the nonlinear dynamic motion of beads in a magnetic-field wave [14]. The traveling wave is produced by an external rotating field superimposed on an array of microferromagnets. It was shown to the first-order approximation that bead motion can be characterized by the equation of motion for an overdamped nonlinear harmonic oscillator [8], at least in the phase-locked regime. In the phase-slipping regime, on the other hand, the nonlinear harmonic-oscillator equation does not adequately capture the fascinatingly rich experimental behavior.

The goal of this work is to shed light on the phase-slipping regime of motion, and in particular, investigate how the bead motion changes when higher-order terms in the forcing function are retained. In these investigations, we attempt to answer questions such as the following: are bounded orbits possible from the coupling between additional higher-order forcing terms? How does the critical frequency depend on the higher-order terms and other system parameters? What different types of subharmonic motions are observed as a result of the interplay of higher-order terms? Due to the complicated nature of the forcing functions, the solutions must be determined numerically and, in this case, were solved using classical discretization schemes for the motion of a bead in a one-dimensional (1D) traveling wave.

In these investigations, we have restricted our attention to the deterministic transport of magnetic beads above a 1D periodic array of magnetic line poles. As such, the results from these simulations must be interpreted as a limiting approximation for the weak diffusion regime of colloidal motion, which is applicable to systems of colloids larger than 1 μm. For continuity, we will reserve investigations that include noise, such as thermal motion and defects in magnetization patterns, for future work.

The rest of this work is organized as follows. The problem description and computational method is provided in Sec. II. Simulation results are provided in Sec. III and the implications of these results and its relevance to applications in colloidal separation are discussed in Sec. IV. A brief conclusion in Sec. V provides a general overview and possible avenues of future work.

II. COMPUTATIONAL METHOD

The basic concept of traveling-wave magnetophoresis is that the superparamagnetic bead attempts to follow the movement of positions of magnetic-field maxima across a surface. One such example is the 3×3 array of 5 μm cobalt micromagnets picture in Figs. 1(A)–1(D) below, on which a 1 μm superparamagnetic bead labeled as (b) is transported along the positive x direction due to a uniform magnetic field rotating in the xz plane. The combination of the fixed magnetic-field distribution produced by the magnetic microarray and the rotating external field leads to the creation

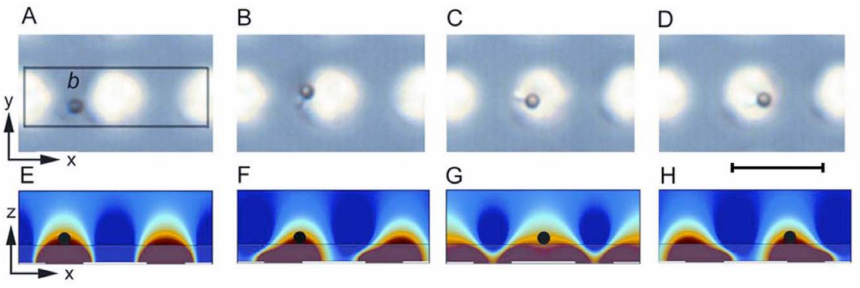

FIG. 1. (Color online) An array of cobalt micromagnets is imaged by reflective light microscopy, and the darkened bead is shown to move in the positive *X* direction by the sequence of images in A–D. The finite element simulations in E–H depict the movement of the locations of magnetic-field maximum (colocated with bead denoted by the black circle) across the micromagnet array. Scale bar is 8 μm.

of a traveling wave of magnetic-field maximum that moves linearly across the substrate. Figures 1(E)–1(H) present a two-dimensional (2D) cross section of the magnetic-field distribution of three micromagnets (delineated by the black rectangle in Fig. 1) as θ is rotated in the xz plane. The superparamagnetic bead has been drawn to scale as a black circle on the finite element simulation at the point of the magnetic-field maximum.

The essential physics of a superparamagnetic bead moving in response to a traveling magnetic-field wave can be captured with the aid of a few reasonable assumptions. In order to simplify the problem, the micromagnets in the array are assumed to be identical both in their shape and direction of permanent magnetization, and arranged in a perfectly crystalline 2D lattice. We further simplify the computation by assuming that the effective pole distribution of the substrate can be expressed in one dimension as an array of magnetic line charges of alternating sign of period d, with effective charge density $\lambda(x)$ given by

$$\lambda(x) = 2\lambda_0 \sum_{n=odd} \cos\left(\frac{2\pi n}{d}x\right), \tag{1}$$

where λ_0 is the effective charge density of the substrate and is an experimentally determined parameter.

The field produced by the substrate can be determined through separation of variables and matching the boundary conditions of Eq. (1). The resulting field of the micromagnet array in combination with the external magnetic field H_{ext} rotating at a driving frequency ω is given by

$$\vec{H} = \begin{bmatrix} H_{ext}\sin(\omega t) - \lambda_0 \sum_{n=odd} e^{-(2\pi n/d)z} \sin\left(\frac{2\pi n}{d}x\right) \\ H_{ext}\cos(\omega t) - \lambda_0 \sum_{n=odd} e^{-(2\pi n/d)z} \cos\left(\frac{2\pi n}{d}x\right) \end{bmatrix}. \tag{2}$$

Once the magnetic field is known everywhere, it is possible to compute the magnetic force on a linearly magnetizable spherical bead using the well-known equation for the force on a point dipole in the presence of a magnetic-field gradient, given by

$$\vec{F} = \mu_0(\vec{m}\cdot\vec{\nabla})\vec{H}, \tag{3}$$

where $\vec{m}=\bar{\chi}V\vec{H}$ is the dipole moment of the bead and is a function of the bead's volume V and the total magnetic field at the bead center, $\vec{H}$. The material properties of the bead, including its magnetic volume susceptibility χ, are accounted for in Eq. (3) including corrections for the bead's spherical shape, which are collectively incorporated into $\bar{\chi}=3\chi/(\chi+3)$. Inserting Eq. (2) into Eq. (3), the resulting expression of force becomes

$$\vec{F} = \mu_0\bar{\chi}V\lambda_0 H_{ext}\begin{bmatrix} \sum_{n=odd} k_n e^{-k_n z}\sin(k_n x-\omega t) - \frac{\lambda_0}{2H_{ext}}\sum_{n=odd}\sum_{m=odd}(k_n-k_m)e^{-(k_n+k_m)z}\sin[(k_n-k_m)x]\hat{x} \\ \sum_{n=odd} k_n e^{-k_n z}\cos(k_n x-\omega t) - \frac{\lambda_0}{2H_{ext}}\sum_{n=odd}\sum_{m=odd}(k_n+k_m)e^{-(k_n+k_m)z}\cos[(k_n-k_m)x]\hat{z} \end{bmatrix}, \tag{4}$$

where $k_j=2\pi j/d$ represents each of the j spatial wavelengths in the Fourier expansion and resulting summations.

Here, we study the translation of the bead across the substrate as a result of traveling waves moving at different angular velocities. In order to simplify the problem, the motion of the bead in the z direction is ignored, which is a reasonable assumption since the bead remains close to the substrate at all times and the oscillatory motion of the bead in the vertical direction tends to be small. For low Reynold's number systems such as this one, the inertial terms can be ig-

nored, and thus the equation of motion in the overdamped limit becomes

$$\frac{dx}{dt} = \frac{\mu_0 \bar{\chi} V \lambda_0 H_{ext}}{6\pi\eta a} \sum_{n=odd} k_n e^{-2\pi n\beta} \sin(k_n x - \omega t) - \frac{\lambda_0}{2H_{ext}} \sum_{n=odd} \sum_{m=odd} (k_n - k_m) e^{-2\pi(n+m)\beta} \sin[(k_n - k_m)x], \tag{5}$$

where the friction coefficient on the particle is assumed to be Stoke's drag on a sphere of radius a in a fluid of viscosity η. Equation (5) assumes that the bead's vertical position is always one radius above the substrate, which allows the exponential terms to be written as a function of the control parameter $\beta = a/d$, which is the ratio between the bead's radius a and the substrate's periodicity d. Hydrodynamic effects due to the bead's proximity to the wall were not taken into account in Eq. (5); however this would result merely in multiplication of Eq. (5) by a constant since the bead's vertical position does not change.

Previously, we demonstrated how this equation can be recast in the form of a nonlinear harmonic oscillator when only the first term in the expansion is retained [14], leading to the result

$$\frac{d\phi}{d\tau} = \sin(\phi) - \frac{\omega}{\omega_c}, \tag{6}$$

where the critical frequency of the system is given by

$$\omega_c = \frac{2\mu_0 \bar{\chi} \lambda_0 H_{ext}}{9\eta} (2\pi\beta)^2 e^{-2\pi\beta}. \tag{7}$$

An exact solution can be obtained for the phase velocity in Eq. (6), and after transformation back into real space, the resulting particle velocity is given by

$$\left\langle \frac{dx}{dt} \right\rangle = \begin{cases} \omega \dfrac{d}{2\pi} & \text{for } \omega \le \omega_c \\ (\omega - \sqrt{\omega^2 - \omega_c^2}) \dfrac{d}{2\pi} & \text{for } \omega > \omega_c \end{cases}, \tag{8}$$

which demonstrates the bifurcation in the velocity vs frequency relationship. That is, when the driving frequency of the rotating field is less than the critical frequency of the system ($\omega \le \omega_c$), then phase-locked motion occurs and the bead travels at the same speed as the traveling wave. Alternatively when the driving frequency is above the critical frequency ($\omega > \omega_c$), then the bead enters the phase-slipping regime characterized by a rocking motion but time-averaged forward progression over all frequencies.

The reason that the critical frequency in expression (7) varies in a complicated manner in β is a result of competing influences in the scaling relationship for magnetic force. On one hand, the magnetic force increases linearly with the particle's volume. On the other hand, the field gradient decays exponentially away from the substrate, leading to the existence of a maximum in the critical frequency relationship. This feature can be used to implement highly efficient separation of beads based on size, as demonstrated experimentally [14].

One unexplained behavior reported experimentally is that for certain frequencies the beads became trapped in bounded orbits (i.e., the beads did not move across the micromagnet array), which contradicts the predictions of Eq. (8) which imply that the bead will have a positive velocity at every frequency. In order to further investigate this discrepancy, we solve the full Eq. (5) numerically using a nondimensional analysis. For convenience, we write the nondimensional velocity of the particle as

$$\frac{d\tilde{x}}{d\tau} = \left\{ \sum_{n=odd} 2\pi n e^{-2\pi n\beta} \sin\left[2\pi \left(n\tilde{x} - \frac{f}{f_N}\tau \right) \right] - \frac{\xi}{2} \sum_{n=odd} \sum_{m=odd} 2\pi(n-m) e^{-2\pi(n+m)\beta} \sin[2\pi(n-m)\tilde{x}] \right\}, \tag{9}$$

and use the following group of renormalization parameters:

$$\tau = f_N t, \quad \tilde{x} = xd, \quad \xi = \frac{\lambda_0}{H_{ext}}, \quad \beta = \frac{a}{d}, \quad f_N = \frac{2\mu_0 \bar{\chi} H_{ext}^2}{9\eta} \xi \beta^2. \tag{10}$$

The velocity vs frequency relationship of the particle is studied as a function of β and ξ using high fidelity numerical integration of the bead's trajectory. Clearly, Eq. (9) contains a combination of forcing terms including dynamic terms occurring in the single summation and static terms occurring in the double summation that only depend on the particle's current position. In order to directly compare the simulations for different values of ξ and β, the critical frequency for each simulation is rescaled to remove the ξ dependence (i.e., $f_N^* = f_N/\xi$). In this way, the ξ dependence is limited to the static terms of Eq. (8), and the effect of modulating ξ is now confined to modulating the effect of static fields on the bead's motion.

III. RESULTS

All simulations were performed in MATHEMATICA. An arbitrarily chosen field strength of $H_{ext} = 10$ Oe is used for all simulations, and the values for the effective bead susceptibility and fluid viscosity are $\bar{\chi} = 0.273$ and $\eta = 0.01$ P in order to reflect the true parameters of the previously analyzed experimental work. The normalization frequency for these simulations is therefore $f_N = 48.229\beta^2$ Hz. The bead's trajectory is analyzed using the NDSolver function and is computed for 10 000 cycles of the external field. The steady-state velocity of the bead is then determined for different values of β and ξ by analyzing the final 70% of the bead's trajectory after which all the initial transient motion is negligible. We confirmed through numerical simulations that the second-order inertial terms are negligible for describing the particle dynamics at these length scales, and the first-order dynamics in Eq. (5) adequately describes the bead's motion.

In the subsequent simulations, the parameter ξ was allowed to vary over 2 orders of magnitude from 0.1 to 10. The

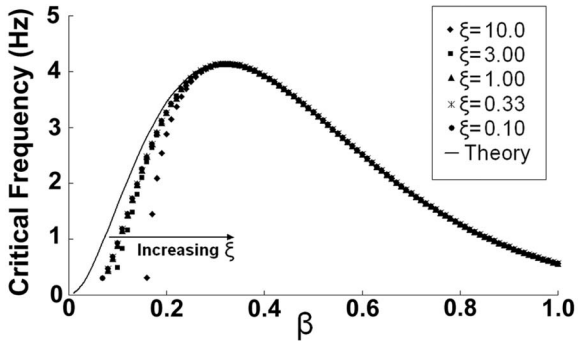

FIG. 2. The critical frequency is plotted as a function of β for different values of ξ.

values of β studied in these simulations ranged from 0.05 to 1.0. The number of harmonics retained in the expansion is $n=100$ for all simulations, which effectively approaches the asymptotic limit for the exact solution of the forcing function produced by an array of line poles for values of $\beta>0.05$.

First, the critical frequency of the system was analyzed for different values of β and ξ and compared to the analytical solution for the critical frequency (7) in which only a single harmonic is retained. The results illustrated in Fig. 2 indicate that for large bead sizes ($\beta>0.3$), the higher-order harmonics in the forcing function can be justifiably ignored, as the simulation results closely matches the first-order theoretical model of Eq. (7). However, for lower values of β, the critical frequency diverges from the analytical result and is more pronounced for larger values of ξ. In the small β range, the curves are nearly identical for $\xi<1$; however for $\xi>1$ the critical frequency shifts more dramatically to lower values and the cutoff frequency for which beads can no longer move shifts to higher values of β.

The velocity vs frequency relationships for values of β in the range of 0.10–0.24 are provided in Fig. 3(a). Clearly, at higher values of β, the mobility of the beads reduces to the first-order nonlinear harmonic oscillator of Eq. (6). For lower values of β, the bead appears to lock into certain characteristic ratios for its relative velocity in comparison with the velocity of the traveling wave. This effect is clearly observed in Fig. 3(b) and appears to be integer multiple ratios, such as 1/3, 1/2, 1/5, 1/7, 3/5, and others, which are listed here in order of its population frequency within the spectrum of motion. The trajectories associated with each of these subharmonic modes of motion are provided in Fig. 4. Effectively, the bead attempts to lock into subharmonic orbits, with the most dominant coupling strength occurring between the first and third harmonics of the forcing function. The coupling strength, characterized by the degree to which the bead has a particular velocity, appears to decrease for the higher-order harmonics. This general type of intermittent staircase behavior is reminiscent of the devil's staircase, which has been observed in other nonlinear dynamical systems [2–7], and also has some similarities with fractal relationships, such as the Cantor function [18].

A histogram of this subharmonic locking effect can be observed in the 2D surface plot provided in Fig. 5, in which the relative population frequency of each characteristic integer multiple is plotted as a function of β. As β increases, the

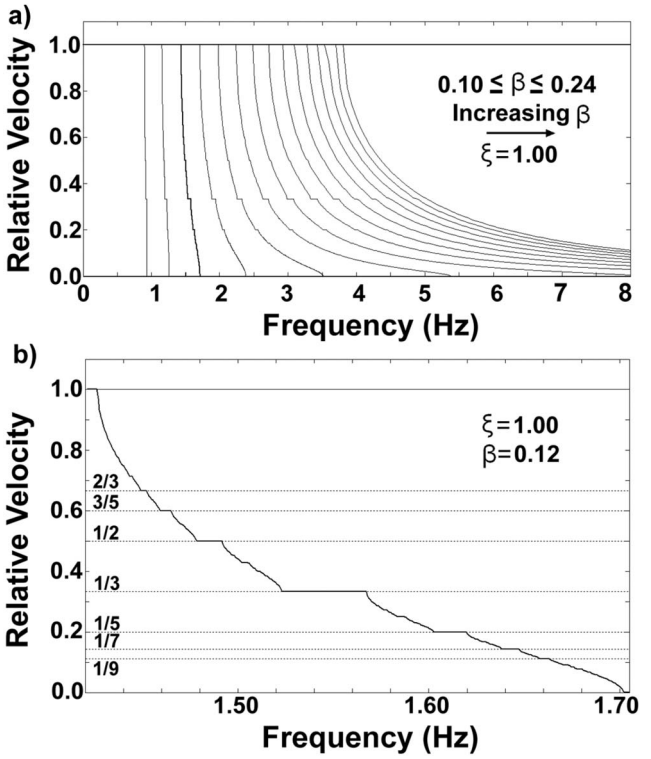

FIG. 3. (a) The velocity vs frequency relationships are depicted as a function of β assuming $\xi=1.0$. (b) An expanded view for $\beta=0.12$ is depicted, clearly showing the quasiperiodic locking that occurs near integer multiple ratios for the bead's relative velocity.

subharmonic locking is dramatically reduced, and the bead spends significantly longer percentages of its spectral motion in the lower noninteger multiple velocity distributions, corresponding to behavior described in Eq. (6). For β in the range of 0.10–0.15, however, a majority of the bead's spectral motion is observed at (or near) an integer multiple ratio. Not all of the integer multiple ratios are present for each value of β, and in addition, the relative magnitude of the population density is not constant. For the lowest values of

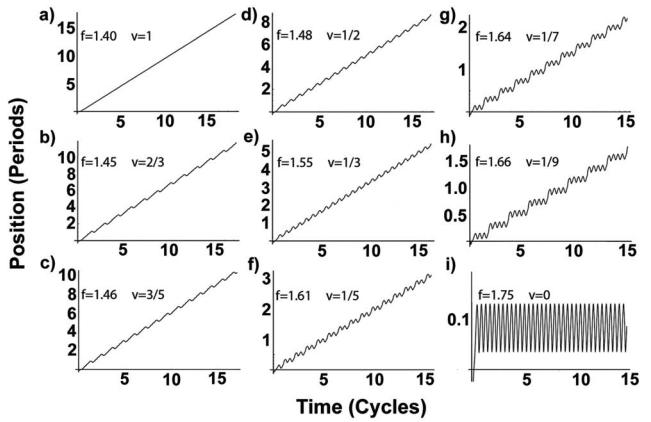

FIG. 4. [(a)–(i)] The trajectory of the bead for $\beta=0.12$ and $\xi=1.0$ is plotted for nine different values of the driving frequency, depicting different types of subharmonics that can be observed in Fig. 3(b).

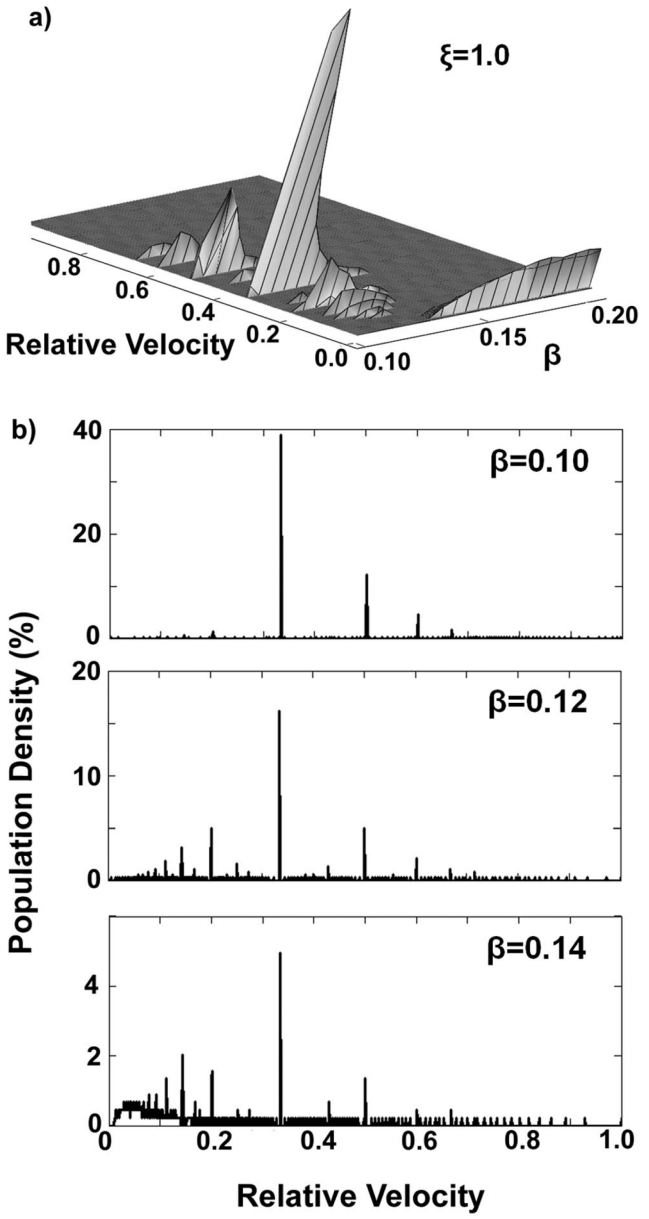

FIG. 5. A 2D surface plot histogram is provided to demonstrate the population frequency of subharmonic locking near different integer multiple ratios of the bead's relative velocity. The dominant peak is located at a relative velocity of 0.333. Three cross sections of the 2D surface plot are provided in (b)–(d) for different values of β. For small β, the majority of the velocity is populated for integer multiple ratios greater than 0.333, and for larger β, the converse is true.

β, the bead populates to a greater extent the integer multiple ratios greater than 0.33. Conversely, for the higher values of β, the bead populates to a greater extent the integer multiple ratios smaller than 0.33. In order to remove the noise of this surface plot, the histogram was processed with a low-pass filter; thus only the major peaks are displayed in Fig. 5.

Another interesting aspect of this system is that the bead's orbit becomes bounded (i.e., velocity becomes zero) for frequencies above what we denote as the "stopping frequency," ω_s, an effect which was also reported experimentally [14]

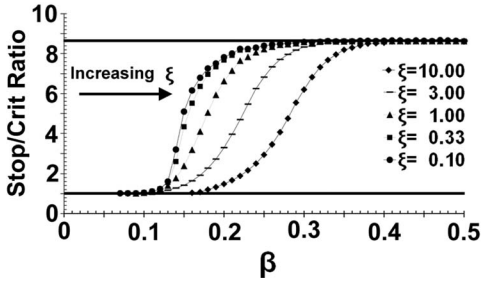

FIG. 6. The ratio between the stopping frequency and critical frequency ω_s/ω_c is presented as a function of β and for different values of ξ. The ratio converges to unity for small values of β and converges to the predictions of Eq. (6) for large values of β. The effect of ξ is to shift the curve to the right.

and cannot be explained by the nonlinear harmonic oscillator of Eqs. (6)–(8). From visual inspection of Fig. 6, it appears that the ratio ω_s/ω_c approaches a limiting value as β increases. It is not always possible to determine ω_s for all values of β, since Eq. (6) does not predict the possibility of spatially bounded motion. In these cases, we implemented an artificial cutoff for the stopping frequency which we assume had occurred once the relative velocity drops below e^{-5} compared with the velocity of the traveling wave. For the nonlinear harmonic oscillator of Eq. (6), this velocity occurs at a characteristic limiting ratio of ω_s/ω_c that approaches 8.629, and it is evident that all curves approach this limiting ratio for sufficiently high values of β. This is further evidence that for large values of β, the bead motion obeys Eq. (6). For lower values of β, on the other hand, ω_s/ω_c asymptotically approaches unity for all values of ξ. Like before, the effect of the substrate's static contribution to the forcing term (i.e., the effect of ξ) is to shift the entire curve to the right, such that only larger beads are able to move in the traveling wave.

IV. DISCUSSION

The intent of these simulations was to investigate the complex motion of magnetic beads above magnetic crystalline lattices and to determine how the driving frequency of a rotating magnetic field affects the bead's mobility for potential applications in colloidal separation. The results of Fig. 2 indicate that there exists a critical bead size which can experience the fastest velocity in a traveling wave or in other words has the highest critical frequency. The location of this critical bead size can be determined by evaluating the solution to $d\omega_c/d\beta=0$, which in this case occurs at $\beta=\pi^{-1}$ and is consistent with the location shown in Fig. 2. This finding suggests that a polydisperse set of beads can be size sorted by scanning the frequency from high to low, only when the range of β does not exceed 0 to π^{-1}.

Much of the initial impetus for this work also originated from unexplained experimental observations, in which magnetic beads appeared to become trapped in bound orbits at frequencies only slightly above the critical frequency of the system. This behavior differs dramatically from the predictions of Eqs. (6)–(8) and suggests the possibility of infinite separation resolution between beads of different size in the

sense that at certain frequencies some beads will have bound orbits whereas the orbits of others are unbounded. Let us take a specific example analyzed in our previous work of a micromagnet array having 8 μm periodicity and containing a polydisperse suspension of magnetic beads ranging from 1 to 5 μm in diameter. If a driving frequency of 3.5 Hz is applied to the system, then the beads larger than about 3.2 μm (i.e., $\beta=0.2$) will be phase locked with the traveling wave and move at 28 μm/s, whereas the beads smaller than 3.2 μm will be in the phase-slipping regime and will move less quickly or not at all. From inspection of Fig. 3(a), it is clear that beads in the range of 1.00–2.25 μm diameters will be trapped in bound orbits and will never advance to the next magnet in the traveling wave, whereas beads in the range of 2.25–3.2 μm will move with different velocities which increase with the bead size. This behavior is qualitatively similar to what has previously been reported [14].

These simulations also serve as an important guideline for improving the separation apparatus. The highest separation resolution is achieved by working with the lower range of β, in this case between 0.10 and 0.15, where ω_s/ω_c approaches unity. This ratio is illustrated in Fig. 6 and suggests that for this range of β, the separation apparatus operates as an ideal high-pass filter—only beads above a certain size can translate across the array, whereas smaller beads cannot.

Scanning the frequency is not the only control parameter that can be applied to implement size sorting. Increasing the strength of the rotating field (i.e., reducing ξ) can also affect the mobility of the beads; however this parameter is sensitive only to small β values and may not be a viable solution for most separation apparatus for fear of remagnetizing the micromagnets in higher field strengths.

Finally, it is also conceivable that an array of micromagnets whose periodicity increases along the direction of bead motion (i.e., commensurately increasing the magnet size and spacing d) can also achieve very effective separation. In fact, the movement of beads in a system of gradually increasing magnet spacing is predicted to result in localization of beads into separated bands, much similar to gel electrophoresis of DNA, proteins, and other charged biological molecules.

V. CONCLUSION

The goal of this work was to study the fascinating nonlinear behavior of magnetic beads exposed to a superposition of forward traveling waves of different spatial frequencies. The results indicate that a large range of additional dynamic modes is possible in this system, including subharmonic phase locking, and the possibility of bounded orbits at finite frequencies, which is not possible for bead motion of a single harmonic traveling wave. These results have important ramifications in the field of colloidal separation and support the conjecture that "infinite separation resolution" can be achieved between two bead types which have only minor differences in their size, shape, or material properties. This work also captures the essence of the unexplained experimental behavior previously reported by one of the authors [14]; however a quantitative comparison still requires some additional work. For future comparison of theory and experiment, a more accurate 2D representation for the magnetic pole distribution is required. In this case, the possibility of additional directions of motion and possibly stochastic effects are expected to further enrich the wide range of physically interesting behavior, including new quasiperiodic locking modes and other nonlinear dynamical behavior.

ACKNOWLEDGMENT

The authors are grateful for the support of this work from the National Science Foundation (Grant No. CMMI 0800173).

[1] O. Pierre-Louis and M. I. Haftel, Phys. Rev. Lett. **87**, 048701 (2001).
[2] J. Wiersig and K.-H. Ahn, Phys. Rev. Lett. **87**, 026803 (2001).
[3] S. E. Brown, G. Mozurkewich, and G. Grüner, Phys. Rev. Lett. **52**, 2277 (1984).
[4] C. Reichhardt and Franco Nori, Phys. Rev. Lett. **82**, 414 (1999).
[5] A. Gopinathan and D. G. Grier, Phys. Rev. Lett. **92**, 130602 (2004).
[6] P. T. Korda, M. B. Taylor, and D. G. Grier, Phys. Rev. Lett. **89**, 128301 (2002).
[7] M. Khoury *et al.*, Phys. Rev. B **78**, 155433 (2008).
[8] S. H. Strogatz, *Nonlinear Dynamics and Chaos: With Applications to Physics, Biology, Chemistry and Engineering* (Addison-Wesley Pub., Reading, MA, 1994).
[9] E. Levi, IEEE Trans. Magn. **9**, 242 (1973).
[10] H. W. Lee, K. C. Kim, and J. Lee, IEEE Trans. Magn. **42**, 1917 (2006).
[11] N. G. Green and H. Morgan, J. Phys. D **30**, 2626 (1997).
[12] L. Cui, D. Holmes, and H. Morgan, Electrophoresis **22**, 3893 (2001).
[13] Y. Roichman, V. Wong, and D. G. Grier, Phys. Rev. E **75**, 011407 (2007).
[14] B. B. Yellen *et al.*, Lab Chip **7**, 1681 (2007).
[15] A. Soba, P. Tierno, T. M. Fischer, and F. Sagues, Phys. Rev. E **77**, 060401 (2008).
[16] P. Tierno *et al.*, J. Phys. Chem. B **111**, 13479 (2007).
[17] M. Wiklund *et al.*, Lab Chip **6**, 1537 (2006).
[18] R. L. Devaney, *An Introduction to Chaotic Dynamical Systems* (Addison-Wesley, Redwood, CA, 1987).